Fringe contrast enhancement of digital off-axis hologram via sparse representation

Yuan Hong (洪 源), Tielin Shi (史铁林), Yichun Zhang (张贻春), and Guanglan Liao (廖广兰)*

State Key Laboratory of Digital Manufacturing Equipment and Technology, Huazhong University of Science and Technology, Wuhan 430074, China

**Corresponding author: guanglan.liao@hust.edu.cn*

Received November 28, 2015; accepted March 11, 2016; posted online April 26, 2016

This Letter presents a novel approach to enhance the fringe contrast (visibility) in a digital off-axis hologram digitally, which can save several adjustment procedures. In the approach, we train a pair of coupled dictionaries from a low fringe contrast hologram and a high one of the same specimen, use the dictionaries to sparse code the input hologram, and finally output a higher fringe contrast hologram. The sparse representation shows good adaptability on holograms. The experimental results demonstrate the benefit of low noise in a three-dimensional profile and prove the effectiveness of the approach.

OCIS codes: 090.1995, 100.2980.

doi: 10.3788/COL201614.060901.

Conventional digital holography can be divided into two main types: in-line digital holography[1], and off-axis digital holography[2,3]. In the presence of zero-order and conjugate images, in-line digital holography usually requires two[4,5] or three[6] phase-shifting holograms to extract the desired information. This leads to the complexity of the optical configuration and the restriction on dynamic applications. Different from the in-line condition, off-axis digital holography overcomes these shortcomings because it needs only one single exposure. The main idea of the off-axis configuration is that the zero order, first order and −1 order of diffraction can be separated from each other in the angular spectrum of the hologram. By filtering the associated spatial frequencies, the zero-order and conjugate image can be eliminated[7]. Since the fringe contrast in the hologram affects the diffraction efficiency of −1 order, the reconstructed three-dimensional (3D) profile has more serious disturbances when the contrast is lower. In practice, with the change of the objective lenses, the reflectivity of different samples, etc., researchers need to adjust the optical path difference (OPD) and the object-to-reference intensity ratio or even to employ a longer coherence length light source to increase the visibility of the fringes. The operations mentioned above take up much time in preparing a high-quality hologram, which obviously reduces the measurement efficiency. Researchers need a novel technique to increase the visibility digitally.

Sparse representation[8] has already been introduced in image processing and pattern recognition, etc. These applications are based on the assumption that the signal can be sparsely represented according to the compressive sensing (CS) theory[9,10]. Efforts have been made to employ this tool in the digital holography field[11–13]. Katkovnik *et al.*[14,15] utilized the sparse coding of the amplitude and absolute phase to reconstruct the wavefront in phase-shifting interferometry and digital off-axis holography. Memmolo *et al.* proposed a refocusing criterion via sparsity measurements in digital holography[16]. They also presented a sparsity denoising method of digital holograms without knowing the noise statistics[17], in which the speckle noise n_s and the additive noise n_a were supposed to corrupt the digital hologram H. Here, n_s is assumed as a multiplicative uniform noise, and n_a is modeled by zero-mean Gaussian noise. In consideration of the degree of the coherence γ, the hologram with noise can be written as

$$H = |O|^2 + |R|^2 + 2|OR||\gamma| \cos(\varphi + n_s) + n_a, \quad (1)$$

where O is the object light field, R is the reference light field, and φ stands for the phase difference between O and R.

In this Letter, we focus on enhancing the fringe contrast via sparse representation in holograms that are recorded directly by the imaging sensor in digital off-axis holography. Although the zero order ($|O|^2 + |R|^2$) in Eq. (1) can be suppressed[18,19], it is not appropriate to improve the contrast of the pixel values directly in the presence of n_a. The method we used is based on the coupled dictionary training technique, which has been used for image super-resolution[20]. We record a high fringe contrast hologram and a low fringe contrast hologram of the same sample to train a couple of dictionaries. The image patches in the holograms are approximated by a sparse linear combination of the dictionary atoms.

The experiments were conducted on an improved Mach–Zehnder interferometer optical system, as shown in Fig. 1(a), where the sample was a 1951 USAF resolution test target. Since the reflected object light intensity influences the visibility (contrast) in the hologram, the non-uniform reflectivity of the sample should be considered as well. The test target just contains both the high

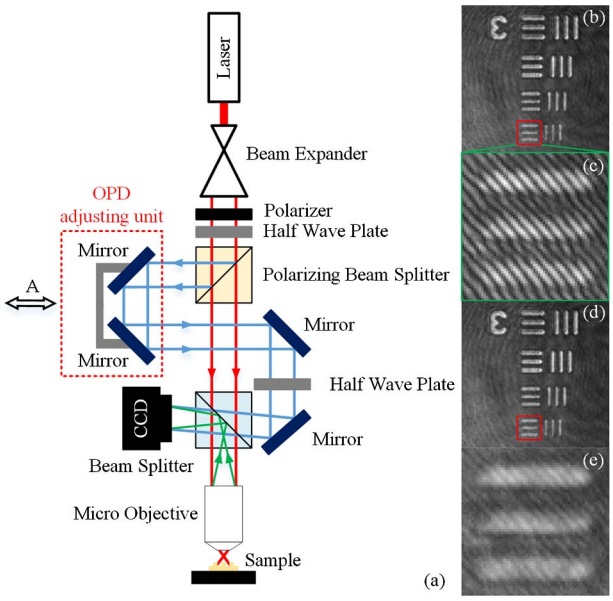

Fig. 1. (a) Experimental setup for reflective off-axis digital holography, (b) highest fringe contrast hologram X_t, (c) local zoom of (b), (d) lowest fringe contrast hologram Y_t, and (e) local zoom of (d).

reflectivity patterns (chromium film) and the low reflectivity background (glass). An additional adjusting unit (indicated by red dashed box in Fig. 1(a)) was inserted to change the OPD between the object and the reference beams. We used a He–Ne laser with a wavelength of 632.8 nm and a coherence length of about 30 cm. The size of the sensor pixel was 4.65 μm × 4.65 μm, and the 20× objective lens had a numerical aperture of 0.40. By changing the position of the unit along arrow A, we got a series of image-plane holograms with different fringe contrasts.

Next, we prepared a couple of dictionaries D_x and D_y, where D_x is the dictionary of high contrast space and D_y is the dictionary of low contrast space. The holograms with the highest and the lowest contrast were selected for training, as shown in Figs. 1(b) and 1(d), where the areas in the red squares are enlarged in Figs. 1(c) and 1(e), respectively, to show their difference in fringe contrast. The training of the dictionaries is based on the patchwise sparse recovery method[20], where the typical database is one of the key points for specific applications, such as holography. We input two holograms of the same sample: $X_t \subseteq R^n$ with a high fringe contrast and $Y_t \subseteq R^n$ with a low fringe contrast, where R^n represents an n-dimensional real space. To guarantee that the dictionaries are overcomplete, a large number of patches x_j and y_j $(j = 1, ..., N)$ were sampled from X_t and Y_t, respectively. Different from other applications of sparse representation[20], these patches were not "empty" (all pixels are nearly same in an empty patch). We will always observe the interference fringe in the patch, even all pixels of the patch that are background. Because of the mapping from y_j to x_j is unknown and probably nonlinear, we tend to learn the coupled dictionaries with machine learning techniques instead of applying the CS theory immediately. The objective function of training D_x and D_y simultaneously can be expressed as

$$\min_{D_x, D_y} \sum_{i=1}^{N} (\mu \| D_x z_j - x_j \|_2^2 + (1-\mu) \| D_y z_j - y_j \|_2^2), \qquad (2)$$

where $\mu (0 < \mu \le 1)$ balances the reconstruction errors of x_j and y_j, and z_j is the sparse code of x_j and y_j. Since Eq. (2) is highly nonlinear and nonconvex, the dictionary D_x is initialized by standard sparse coding and then fixed while the dictionary D_y is optimized first by a descent method[21]. When D_y is converged, we fix it and then optimize D_x:

$$\begin{aligned} &\min_{D_x} \sum_{i=1}^{N} \| D_x z_j - x_j \|_2^2 \\ &\text{s.t. } z_j = \arg \min_{\alpha} \| y_j - D_y \alpha \|_2^2 + \lambda \| \alpha \|_1, \qquad i = 1, ..., N \\ &\| D_x(:, k) \|_2 \le 1, \qquad k = 1, ..., K. \end{aligned} \qquad (3)$$

where λ is the Lagrangian and $D_x(:, k)$ is the kth column of D_x. The objective function together with the inequality constraint function in Eq. (3) is quadratic, which is a quadratically constrained quadratic program problem[22] and can be solved by using a conjugate gradient descent[23].

After training the dictionaries D_x and D_y for the coupled spaces, we can start to enhance the fringe contrast of the input hologram Y. The hologram patch y_i $(i = 1, ..., N)$ is extracted from Y with insufficient fringe contrast, and $x_i \in X$ is supposed to be the desired patch with high contrast. Our goal is to acquire the high contrast patches x_i in terms of D_x with the formula

$$x_i = D_x \alpha. \qquad (4)$$

The sparse representation α also satisfies the similar relation between the given low contrast patches y_i and the dictionary D_y:

$$y_i = D_y \alpha. \qquad (5)$$

As described in Ref. [24], the issue of calculating α is known as the Lasso[25], which can be formulated as

$$\min_{\alpha} \| D_y \alpha - y_i \|_2^2 + \lambda \| \alpha \|_1. \qquad (6)$$

Since the degree of approximation to y_i (evaluated by the square of the l_2 norm $\| D_y \alpha - y_i \|_2$) and the sparsity of α (represented by the l_1 norm $\| \alpha \|_1$) need to be balanced, the Lagrangian λ is introduced, which means a weighting of the smoothing property; it influences the ability to tolerate n_a on some level. Before solving Eq. (6), we must consider the reasonability of using the image patches directly. For holograms, the main feature is the interference fringe, which indicates that the differences between adjacent

pixels are directional. We extract the normalized gradient feature (x_i' and y_i') for each patch (x_i and y_i) to eliminate the influences of uneven illumination. Hence, y_i in Eq. (6) is replaced by y_i'. After solving Eq. (6), we substitute α into $x_i' = D_x\alpha/\|D_x\alpha\|_2$ and get x_i'. The high fringe contrast hologram patch x_i is then acquired from its normalized gradient feature x_i'. However, compatibility may occur between the adjacent patches. Recovering each high contrast patch individually may result in the discontinuity of the interference fringe. Thus, we partially overlap the pixels of the adjacent patches when extracting and restoring them and average the values of the overlapped area. The algorithm is summarized in Fig. 2.

We set the dictionary size K to 512 and input the training images X_t and Y_t. Then, $N = 15000$ patches pairs are sampled from X_t and Y_t. Each patch is 10×10, according to the period of the interference fringes. The same parameters are used in the fringe contrast enhancement procedures as well. The parameter λ is set to 0.1 when computing sparse coefficients. We take the mean value m of the patch y_i and extract the normalized gradient feature by $y_i' = (y_i - m)/\|y_i - m\|_2$. Accordingly, the high fringe contrast patch x_i is recovered by $x_i = x_i' \cdot \|y_i - m\|_2 + m$. The training for the dictionaries is executed in MATLAB and takes about 28 min on a personal computer (Intel i5-3230M, 2.60 GHz CPU, 4GB RAM) without using a GPU or parallel processing (only one core was utilized). The enhancement of a 512×512 pixels hologram takes 19.8 s in average.

There are two principal differences in our approach. First, our target is to enhance the fringe contrast in an off-axis hologram. Second, the two images we used for dictionary training are the holograms recorded directly by the camera in digital off-axis holography and have the highest and lowest fringe contrast. We do not need to care about the effect of magnification, as described in Ref. [20]. The training images they used are a high resolution image and a low resolution image, where the high resolution image is blurred, downsampled, and then upscaled by bicubic interpolation to obtain the low resolution image.

Figures 3(a1) and 3(c1) are the original holograms of the 1951 USAF resolution test target that recorded different parts of Fig. 1(b). Both of the holograms havea relatively lower fringe contrast than X_t. The enhanced holograms are exhibited in Figs. 3(b1) and 3(d1). To prove the effectiveness of our algorithm, the regions in the red squares of Figs. 3(a1)–3(d1) are magnified in Figs. 3(a2)–3(d2). We can clearly observe that the fringe

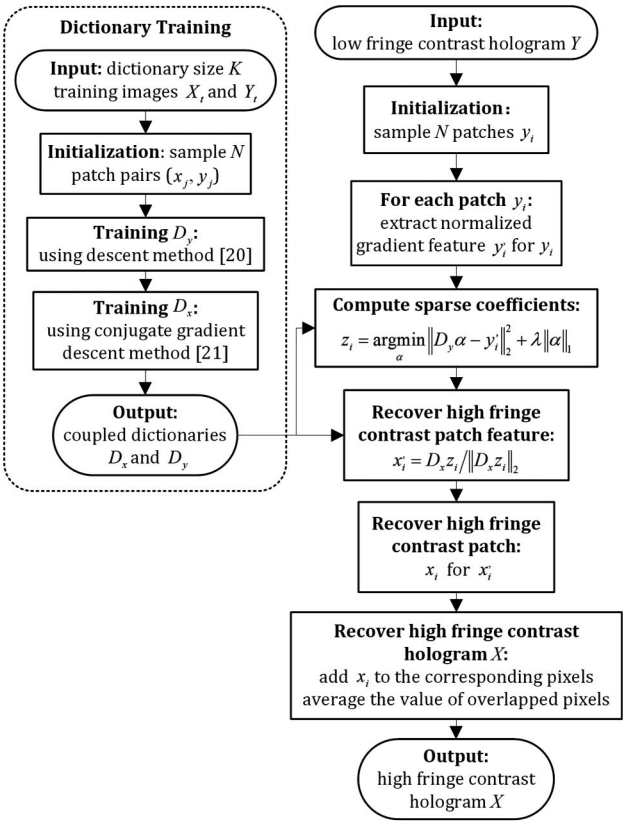

Fig. 2. Fringe contrast enhancement algorithm of digital off-axis hologram via sparse representation.

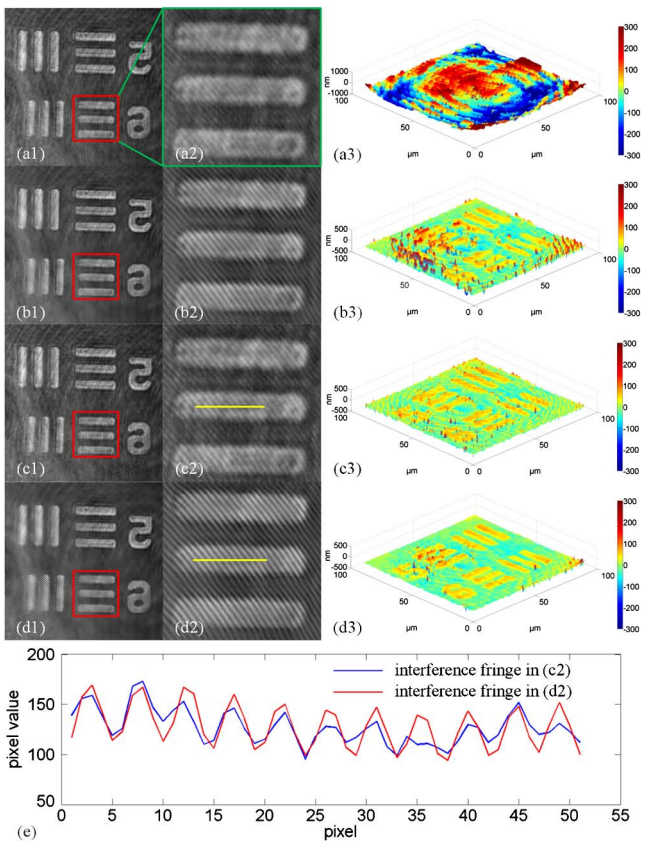

Fig. 3. Comparison of the recorded holograms and enhanced holograms of a different part on 1951 USAF resolution test target: (a1) recorded hologram, (a2) local zoom of (a1), (a3) 3D profile of (a1); (b1) enhanced hologram of (a1), (b2) local zoom of (b1), (b3) 3D profile of (b1); (c1) recorded hologram with higher contrast than (a1), (c2) local zoom of (c1), (c3) 3D profile of (c1); (d1) enhanced hologram of (c1), (d2) local zoom of (d1), (d3) 3D profile of (d1); (e) pixels value of lines indicated by yellow lines in (c2) and (d2).

contrast in the enhanced holograms is much higher than that in the original holograms. The corresponding 3D profiles of the holograms are shown in Figs. 3(a3)–3(d3). The angular spectrum filtering, phase unwrapping, and aberration compensation of the holograms are operated in the same way[26]. Apparently, the 3D profiles of the enhanced holograms have less noise. Especially in Fig. 3(a3), the noise is too heavy to get a correct unwrapping result, while in Fig. 3(b3), it is possible to observe the pattern with our algorithm. The fringe contrast in Fig. 3(c1) is a little higher than that in Fig. 3(a1), leading to a better 3D reconstruction, as shown in Fig. 3(c3). The improvement can be seen as well in Fig. 3(d3). In Fig. 3(e), the blue line stands for the pixels value of the section indicated by the yellow line in Fig. 3(c2), and the red line represents the pixels value of the section indicated by the yellow line in Fig. 3(d2). We can find that the amplitude of the red line is higher than the blue line. To describe the enhancement of the algorithm quantitatively, we calculate the visibility of interference fringes by Fourier analysis[27].

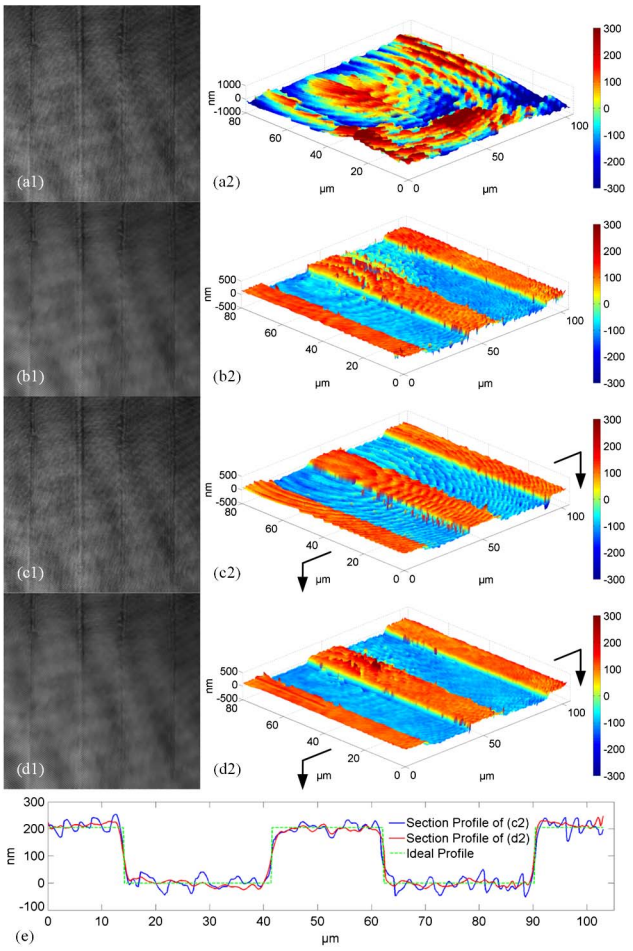

Fig. 4. Comparison of the recorded holograms and enhanced holograms of a groove plate: (a1) recorded hologram, (a2) 3D profile of (a1); (b1) enhanced hologram of (a1), (b2) 3D profile of (b1); (c1) recorded hologram with higher contrast than (a1), (c2) 3D profile of (c1); (d1) enhanced hologram of (c1), (d2) 3D profile of (d1); (e) profiles of the same section in (c2) and (d2).

The visibility of the sections in Figs. 3(c2) and 3(d2) are 0.115 and 0.204, respectively, verifying the effectiveness of the algorithm by the enhancement of 77.4%.

For further verification, we introduce a groove plate that has a groove depth of 200 ± 5 nm as another sample. The dictionaries stay the same to indicate the applicability of the algorithm, and a similar trend can be noticed in the results, as shown in Fig. 4. Profiles of the sections in Figs. 4(c2) and 4(d2) are plotted in Fig. 4(e) by the blue and red lines, respectively. The ideal profile is expressed by the green dashed line. The red profile is smoother than the blue profile. To evaluate the improvement in 3D reconstruction, we calculate the standard deviation to estimate the noise. The standard deviations of the sections in Figs. 4(c2) and 4(d2) are 24.6 and 18.5, improving about 24.8%.

By observing the holograms for training and testing, we notice that the interference fringes in them are indeed the same type (with the similar period). This is because the interference fringe period depends on the angle between the object beam and the reference beam. Once the off-axis optical system is determined, the holograms acquired by the system are almost the same type. The concentric fringes in Figs. 3(a3) and 4(a2) come from the residual wrapped phase due to their frustrated unwrapping processes. The concentric fringes in Fig. 4(c2) come from ghost images, which are components of the zero order in the angular spectrum. The signal-to-noise ratio (+1 order to 0 order ratio) reduces as the fringe contrast decreases.

Therefore, the sparse representation based on the coupled dictionary training technique provides a novel way to enhance the fringe contrast of digital off-axis holography digitally. If enough kinds of image pairs (containing most of the characteristics of the samples to be tested) are obtained for training the dictionaries, the measurement efficiency can be effectively improved by saving the procedures for adjusting the optical system.

References

1. G. Pedrini, P. Fröning, H. Fessler, and H. J. Tiziani, Appl. Opt. **37**, 6262 (1998).
2. E. Cuche, P. Marquet, and C. Depeursinge, Appl. Opt. **39**, 4070 (2000).
3. J. Zheng, P. Gao, B. Yao, T. Ye, M. Lei, J. Min, D. Dan, Y. Yang, and S. Yan, Photon. Res. **2**, 87 (2014).
4. C. S. Guo, B. Sha, Y. Y. Xie, and X. J. Zhang, Opt. Lett. **39**, 813 (2014).
5. Y. Awatsuji, T. Tahara, A. Kaneko, T. Koyama, K. Nishio, S. Ura, T. Kubota, and O. Matoba, Appl. Opt. **47**, D183 (2008).
6. Y. Awatsuji, A. Fujii, T. Kubota, and O. Matoba, Appl. Opt. **45**, 2995 (2006).
7. E. Stoykova, H. Kang, and J. Park, Chin. Opt. Lett. **12**, 060013 (2014).
8. Z. Zhang, Y. Xu, J. Yang, X. Li, and D. Zhang, IEEE Access **3**, 490 (2015).
9. M. Elad, *Sparse and Redundant Representations* (Springer, 2010).
10. M. Elad, M. A. T. Figueiredo, and Y. Ma, Proc. IEEE **98**, 972 (2010).
11. Y. Rivenson, A. Stern, and B. Javidi, Appl. Opt. **52**, A423 (2013).

12. X. Cao, X. Sang, Z. Chen, Y. Zhang, J. Leng, N. Guo, B. Yan, J. Yuan, K. Wang, and C. Yu, Chin. Opt. Lett. **12**, 080901 (2014).
13. M. Sha, J. Liu, X. Li, and Y. Wang, Chin. Opt. Lett. **12**, 060023 (2014).
14. V. Katkovnik, I. A. Shevkunov, N. V. Petrov, and K. Egiazarian, Opt. Lett. **40**, 2417 (2015).
15. V. Katkovnik and J. Bioucas-Dias, J. Opt. Soc. Am. A **31**, 1801 (2014).
16. P. Memmolo, M. Paturzo, B. Javidi, P. A. Netti, and P. Ferraro, Opt. Lett. **39**, 4719 (2014).
17. P. Memmolo, I. Esnaola, A. Finizio, M. Paturzo, P. Ferraro, and A. M. Tulino, Opt. Express **20**, 17250 (2012).
18. C. Liu, Y. Li, X. Cheng, Z. Liu, F. Bo, and J. Zhu, Opt. Eng. **41**, 2434 (2002).
19. T. M. Kreis and W. P. O. Jüptner, Opt. Eng. **36**, 2357 (1997).
20. J. Yang, Z. Wang, Z. Lin, S. Cohen, and T. Huang, IEEE Trans. Image Process. **21**, 3467 (2012).
21. J. Yang, K. Yu, and T. Huang, in *Proceedings of IEEE Conference on Computer Vision and Pattern Recognition* (IEEE, 2010), pp. 3517.
22. S. Boyd and L. Vandenberghe, *Convex Optimization* (Cambridge University Press, 2004).
23. H. Lee, A. Battle, R. Raina, and A. Y. Ng, in *Advances in Neural Information Processing Systems* (2006), pp. 801.
24. J. Yang, J. Wright, T. S. Huang, and Y. Ma, IEEE Trans. Image Process. **19**, 2861 (2010).
25. R. Tibshirani, J. Roy. Statist. Soc. B **58**, 267 (1996).
26. X. Wang, W. Gong, F. Liu, and H. Wang, Proc. SPIE **7848**, 78482X (2010).
27. J. Pomarico and R. Torroba, Optik **95**, 152 (1994).